International Journal of Minerals, Metallurgy and Materials
Volume 21, Number 11, November 2014, Page 1062
DOI: 10.1007/s12613-014-1010-x

Effect of magnesium addition on inclusions in H13 die steel

Zheng Wu, Jing Li, Cheng-bin Shi, and Liang-liang Wang

State Key Laboratory of Advanced Metallurgy, University of Science and Technology Beijing, Beijing 100083, China

(Received: 4 June 2014; revised: 4 July 2014; accepted: 8 July 2014)

Abstract: The effect of magnesium addition on the number, morphology, composition, size, and density of inclusions in H13 die steel was studied. The results show that the total oxygen content in the steel can be significantly decreased to 0.0008wt%. Al_2O_3 and MnS inclusions are changed into nearly spherical $MgO·Al_2O_3$ spinel and spherical MgO·MgS inclusions, respectively. The number of inclusions larger than 1 μm decreases and the number of inclusions smaller than 1 μm increases with increasing magnesium content. V(N,C) precipitates around $MgO·Al_2O_3$ and MgO·MgS inclusions during solidification of liquid steel. The densities of $MgO·Al_2O_3$ spinel inclusions are lower than that of alumina inclusions. With increasing magnesium content in the Mg-containing inclusions, the density of inclusions decreases, leading to the improvement of inclusion removal efficiency.

Keywords: die steel; inclusions; magnesium; deoxidation; thermodynamics

1. Introduction

As one of the widely used hot die steels, H13 die steel is mainly used in forging dies, hot extrusion dies, and nonferrous-metal die-casting molds [1–3]. Because H13 die steel is generally used at high temperature and high pressure and under greater impact working conditions, a higher thermal fatigue performance is required. One of the most important factors affecting the life of H13 die steel is the presence of inclusions [4], especially brittle inclusions, which likely cause intense stress concentration in the steel matrix [5–6]. Therefore, the number, morphology, and size of inclusions in H13 steel should be controlled.

Seo *et al*. [7] studied deoxidation equilibria in liquid iron equilibrated with $MgO·Al_2O_3$ spinel by adding Fe–Al and Ni–Mg alloys and examined conditions for the formation of $MgO·Al_2O_3$ spinel during deoxidation. However, they did not provide a detailed description of the effect of deoxidation by Fe–Al and Ni–Mg alloys on the characteristics of inclusions. Takata *et al*. [8] and Luo *et al.* [9] reported that magnesium treatment can not only decrease the dissolved oxygen content in liquid steel but can also change elongated or tufted Al_2O_3 inclusions into fine and dispersed $MgO·Al_2O_3$ spinel inclusions. The size of the $MgO·Al_2O_3$ spinel inclusions can be controlled to be 5 μm or less [10]; inclusions of this size have no effect on the mechanical properties of steel. In this paper, the effect of magnesium treatment on the number, morphology, size, and composition of inclusions was studied to extend the application of magnesium in the production of high-performance H13 die steel.

2. Experimental

2.1. Experimental materials

The experimental material was H13 scrap steel; its chemical composition is listed in Table 1. High-basicity slag was used for refining in the experiments. The composition of the slag is given in Table 2. The chemical composition of the Mg–Al–Fe alloy is shown in Table 3.

Table 1. Chemical composition of H13 die steel wt%

C	V	Cr	Al	Si	Mn	S	Mo
0.37	0.99	5.05	0.01	1.02	0.27	0.015	1.17

Table 2. Chemical composition of the refining slag wt%

CaO	SiO_2	MgO	Al_2O_3	CaF_2
50	10	8	25	7

Corresponding author: Zheng Wu E-mail: wuzhengnihao@126.com

Table 3. Chemical composition of the Mg–Al–Fe alloy wt%

Mg	Al	Fe
10.02	35.13	54.67

2.2. Experimental procedure

Experiments were performed using a 10-kg ZG-0.01-type vacuum induction furnace with an inner diameter of 9.5 cm and a magnesia crucible with a depth of 18 cm. Pure aluminum powders were added to the magnesia crucible to ensure an identical amount of aluminum addition into liquid steel. The feeding amounts of the slag, steel material, and Mg–Al–Fe alloy in different experiments are shown in Table 4.

Table 4. Feeding amounts of materials in different experiments g

Exp. No.	H13 steel	Slag	Mg–Al–Fe alloy	Pure aluminum
H1	5940	475	0	8.25
H2	4256	340	8	3.10
H3	6540	523	16	3.50
H4	5038	403	20	0

The refining slag, steel material, and pure aluminum powders were fed into the crucible. Argon gas was blown into the induction furnace to exclude air, and the pressure in the furnace chamber was subsequently decreased to 0.01 Pa using a vacuum pump. Steel samples were collected under vacuum conditions when the steel material was molten. The Mg–Al–Fe alloy was added to liquid steel, and the other four steel samples were sampled at 5-min intervals. Thereafter, the liquid steel was cast into ingots. Steel samples cut from ingots produced in experiments H1, H2, H3, and H4 were designated as E1, E2, E3, and E4, respectively.

The morphology and size of inclusions in the steel samples were observed by scanning electron microscopy (SEM) using a Zeiss SUPRA-55 scanning electron microscope. In addition, the chemical composition of inclusions was determined by energy-dispersive X-ray spectroscopy (EDS). The INCA Feature software was used to analyze the number of inclusions; the examined area of steel samples was 70 mm^2. The total oxygen and total nitrogen content in steel samples were analyzed using an O-N900-type gas analyzer.

3. Results and discussion

3.1. Effect of magnesium on the size and type of inclusions

The inclusion size distribution in steel with aluminum deoxidation and aluminum–magnesium deoxidation is shown in Fig. 1. The inclusion size in steel samples E2, E3 and E4 differ significantly. As evident in Fig. 1, steel sample E1 contains more 4–5-μm inclusions. Samples E2, E3, and E4 contain fewer large inclusions (4–5 μm) and more small inclusions (0–1 μm). With increasing magnesium content in liquid steel, the number of inclusions (1–2 μm, 2–3 μm, 3–4 μm, and 4–5 μm) decreases and the number of harmless inclusions (less than 1 μm) increases.

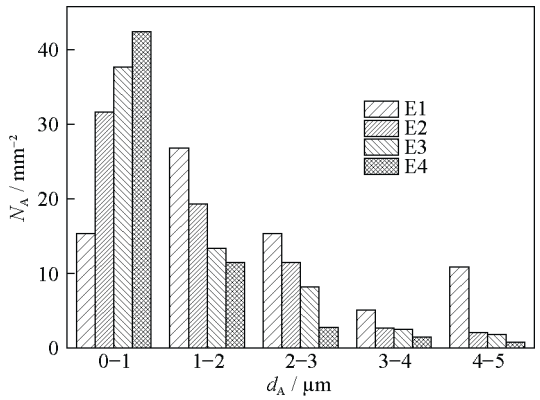

Fig. 1. Inclusion size distribution of steel samples.

The aluminum content in samples E1, E2, E3, and E4 ranges from 0.035wt% to 0.050wt%. The final magnesium content is 0, 0.0007wt%, 0.0010wt%, and 0.0015wt% in samples E1, E2, E3, and E4, respectively. The types of inclusions in the steel samples were determined by SEM-EDS. Typical inclusions in sample E1 are shown in Fig. 2, and typical inclusions in sample E4 are shown in Fig. 3.

Fig. 2 presents SEM images and EDS analysis results of typical inclusions observed in the steel with aluminum deoxidation. Only three types of inclusions were observed. First, the observed inclusions are primarily Al_2O_3 inclusions; their morphologies include triangular, rectangular, and irregular shapes. Second, some complex inclusions were observed in the form of MnS wrapping or adjoining Al_2O_3 inclusions, as shown in Figs. 2(c) and 2(d). The morphology of the MnS inclusion is elongated, as shown in Figs. 2(c) and 2(d). Third, inclusions in the form of an Al_2O_3 core surrounded by an outer V(N,C) layer were observed, as shown in Figs. 2(e) and 2(f). The morphology of the observed V(N,C) inclusions is quadrilateral with clear angularities, as shown in Fig. 2(e). Most of the Al_2O_3 inclusions or complex inclusions observed by SEM-EDS are less than 4 μm in size.

Typical inclusions observed in the steel with aluminum–magnesium deoxidation are shown in Fig. 3. Most of the inclusions are $MgO{\cdot}Al_2O_3$ spinels or, less commonly, $MgO{\cdot}Al_2O_3$ spinels surrounded by an outer V(N,C) layer, as

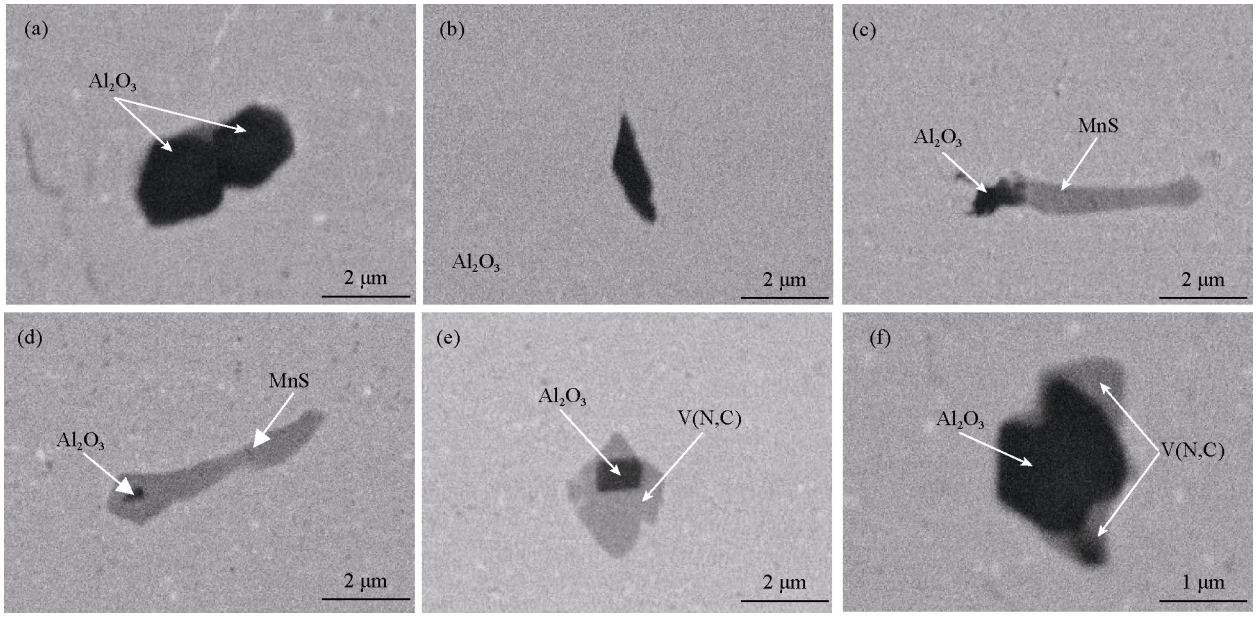

Fig. 2. SEM images and EDS analysis results of typical inclusions observed in sample E1.

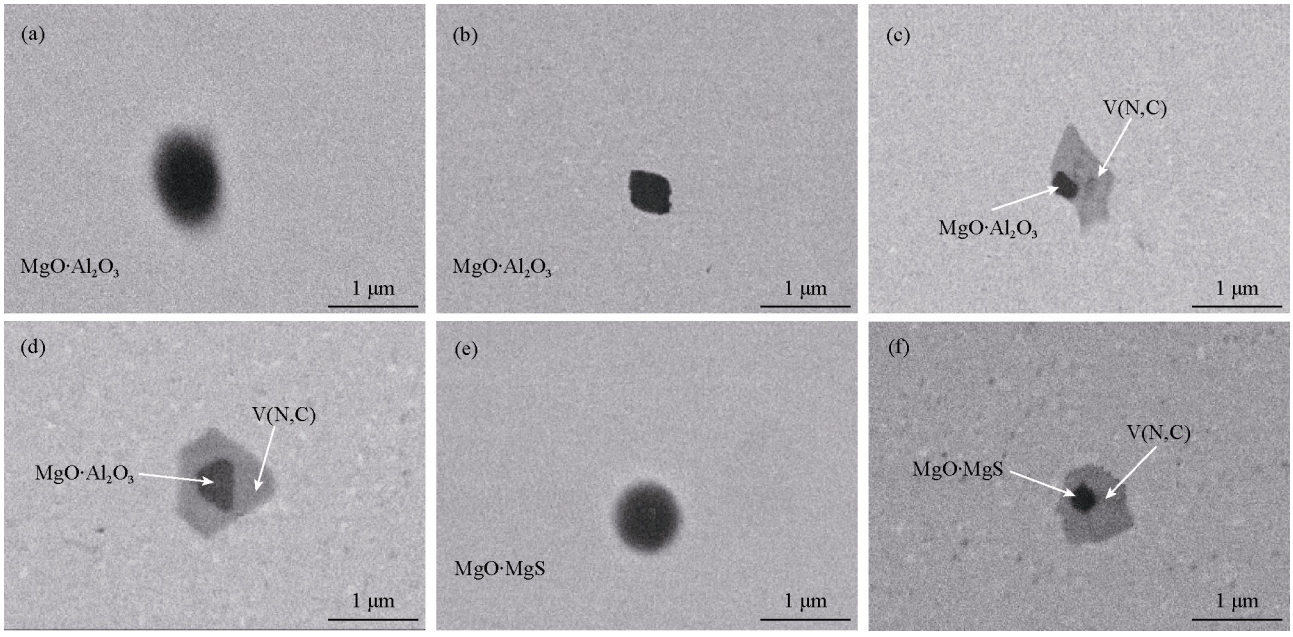

Fig. 3. SEM images and EDS analysis results of typical inclusions observed in sample E4.

shown in Figs. 3(a)–3(d), in addition to a few MgO·MgS inclusions and MgO·MgS inclusions wrapped by V(N,C), as shown in Figs. 3(e) and 3(f). The morphologies of the observed $MgO·Al_2O_3$ spinel and MgO·MgS inclusions are near-spherical. The sizes of the observed $MgO·Al_2O_3$ spinel, MgO·MgS, and complex inclusions are less than 1 μm.

The main reason for this finding is that the added magnesium provided uniform nucleation sites. V(N,C) and MnS precipitate around Al_2O_3 inclusions during solidification of liquid steel with aluminum deoxidation. In contrast, V(N,C) precipitation positions in the steel with aluminum–magnesium deoxidation are the surrounding $MgO·Al_2O_3$ spinel or MgO·MgS inclusions. Compared with the overall dimensions of Al_2O_3 inclusions, those of $MgO·Al_2O_3$ spinel inclusions are smaller, which results in their complex inclusions being smaller.

Thermodynamic analysis was made to evaluate the evolution and modification of oxide and sulfide inclusions. The chemical reaction for the formation of MgS and MnS in liquid steel can be expressed as follows [11–12]:

$$[Mg]+[S]=(MgS),$$

$$\Delta G^{\ominus} = -521470+183.07T, \text{ J/mol} \quad (1)$$

$$\Delta G_1 = \Delta G^{\ominus} + RT\ln\frac{a_{\mathrm{MgS}}}{f_{\mathrm{Mg}}[\%\mathrm{Mg}]\cdot f_{\mathrm{S}}[\%\mathrm{S}]} \quad (2)$$

$$[\mathrm{Mn}]+[\mathrm{S}]=(\mathrm{MnS}),$$

$$\Delta G^{\ominus} = -168822 + 98.87T,\ \mathrm{J/mol} \quad (3)$$

$$\Delta G_2 = \Delta G^{\ominus} + RT\ln\frac{a_{\mathrm{MnS}}}{f_{\mathrm{Mn}}[\%\mathrm{Mn}]\cdot f_{\mathrm{S}}[\%\mathrm{S}]} \quad (4)$$

$$\lg f_i = \sum e_i^j[\%j] \quad (5)$$

where f_{Mg}, f_{Mn}, and f_{S} are the activity coefficients of dissolved magnesium, manganese, and sulfur, respectively, in liquid steel and e_i^j is the first-order interaction coefficient. The first-order interaction parameters used in the present study are listed in Table 5.

The standard state of sulfide is taken as pure solid in Eqs. (2) and (4). By combining Eqs. (1)–(5) with the interaction coefficients, the chemical composition, and the activity of each sulfide in equilibrium, Eqs. (6) and (7) were obtained:

$$\Delta G_1 = -5729\ \mathrm{J/mol} \quad (6)$$

$$\Delta G_2 = 102008\ \mathrm{J/mol} \quad (7)$$

It can be obtained from the changes in the Gibbs free energy term in Eqs. (6) and (7) that the affinity between magnesium and sulfur is greater than that between manganese and sulfur. Magnesium is more likely to participate in the desulfurization reaction at 1873 K because the change in the Gibbs free energy in Eq. (6) was less than 0 J/mol.

Table 5. Interaction coefficients [13–15]

j	C	V	Cr	Al	Si	Mn	S	Mo
e_{Mg}^j	−2.4	—	0.047	—	−0.088	—	−1.38	—
e_{Al}^j	0.091	—	0.0096	0.045	0.0056	0.035	0.030	—
e_{O}^j	−0.450	−0.3	−0.044	−3.9	−0.1310	−0.021	−0.133	0.0035
e_{S}^j	0.111	−0.019	−0.01	0.041	0.0750	−0.026	−0.046	0.0027
e_{Mn}^j	−0.053	0.0057	0.0039	—	−0.0327	0	−0.048	0.0046

In the H2, H3, and H4 experiments, the relationship of magnesium, aluminum, and oxygen contents in liquid steel was determined by the following equation [16]:

$$[\mathrm{Mg}]+2[\mathrm{Al}]+4[\mathrm{O}]=(\mathrm{MgO}\cdot\mathrm{Al_2O_3}),$$

$$\Delta G^{\ominus} = -194430 + 610.25T \quad (8)$$

$$\Delta G = \Delta G^{\ominus} + RT\ln\frac{a_{\mathrm{MgO\cdot Al_2O_3}}}{f_{\mathrm{Mg}}[\%\mathrm{Mg}]\cdot f_{\mathrm{Al}}^2[\%\mathrm{Al}]^2\cdot f_{\mathrm{O}}^4[\%\mathrm{O}]^4} \quad (9)$$

$$\lg f_{\mathrm{Mg}} = \sum(e_{\mathrm{Mg}}^j[\%j] + r_{\mathrm{Mg}}^{\mathrm{O}}[\%\mathrm{O}]^2 + r_{\mathrm{Mg}}^{\mathrm{Mg,O}}[\%\mathrm{Mg}][\%\mathrm{O}] + r_{\mathrm{Mg}}^{\mathrm{Cr,O}}[\%\mathrm{Cr}][\%\mathrm{O}] + r_{\mathrm{Mg}}^{\mathrm{Ni,O}}[\%\mathrm{Ni}][\%\mathrm{O}]) \quad (10)$$

where e_{Mg}^j is the first-order interaction coefficient and $r_{\mathrm{Mg}}^{\mathrm{O}}$, $r_{\mathrm{Mg}}^{\mathrm{Mg,O}}$, $r_{\mathrm{Mg}}^{\mathrm{Cr,O}}$, and $r_{\mathrm{Mg}}^{\mathrm{Ni,O}}$ are the second-order interaction coefficients of Mg. The available second-order interaction parameters are summarized as follows [17]: $r_{\mathrm{Mg}}^{\mathrm{O}} = 3700$, $r_{\mathrm{Mg}}^{\mathrm{Mg,O}} = 48000$, $r_{\mathrm{Mg}}^{\mathrm{Cr,O}} = 0$, and $r_{\mathrm{Mg}}^{\mathrm{Ni,O}} = 1.34$.

The standard state of the oxide is taken as a pure solid phase in Eq. (9). By combining Eqs. (8), (9), and (10) with the interaction coefficients, the chemical compositions, and the activity of $MgO\cdot Al_2O_3$ in equilibrium, Eq. (11) was obtained:

$$[\mathrm{Mg}]\cdot[\mathrm{Al}]^2\cdot[\mathrm{O}]^4 = 5\times10^{-24} \quad (11)$$

According to the literature, when the aluminum content in liquid steel is 0.035wt%–0.050wt% at 1873 K, the dissolved oxygen content is less than 0.0005wt% [10,17]. As shown in Eq. (11), when the aluminum content is 0.035wt%–0.050wt% and the oxygen content is 0.0005wt%, the magnesium content is in the range from 0.00006wt% to 0.00026wt%. The phase-stability diagram of the deoxidation products is shown in Fig. 4. When the aluminum content is 0.035wt%–0.050wt% and the magnesium content is 0.00006wt%–0.00026wt%, the gray area forms, as shown in Fig. 4. Therefore, Al_2O_3 can be transformed into $MgO\cdot Al_2O_3$ under the given conditions. For example, an acid-soluble aluminum content in liquid steel of 0.05wt% and a magnesium content in liquid steel of approximately 0.00013wt% would result in $MgO\cdot Al_2O_3$ generation.

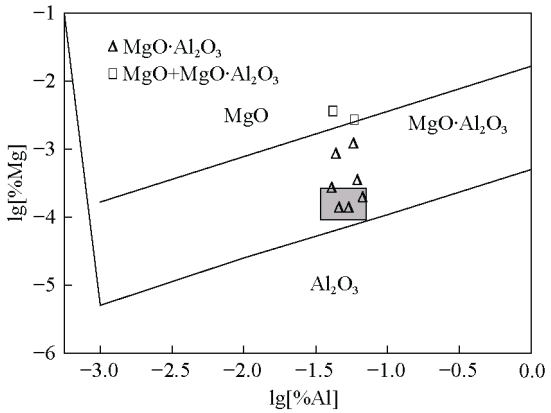

Fig. 4. Phase stability diagram of deoxidation products and experiment results at 1873 K.

3.2. Effect of magnesium on the number of inclusions

The change in the number of inclusions larger than 1 μm

is shown in Fig. 5. As evident in this figure, with increasing experiment time, the number of inclusions in sample E1 decreased. The number of inclusions in samples E2, E3, and E4 were significantly decreased and was less than the number of inclusions in sample E1. With increasing magnesium content in liquid steel, the number of inclusions decreased. For example, in sample E4, the magnesium content in liquid steel was 0.0015wt% and the number of inclusions was 13 mm^{-2}, whereas in sample E2, the magnesium content was 0.0007wt% and the number of inclusions was 32 mm^{-2}. It can be concluded that the number of inclusions decreased with increasing magnesium content in liquid steel.

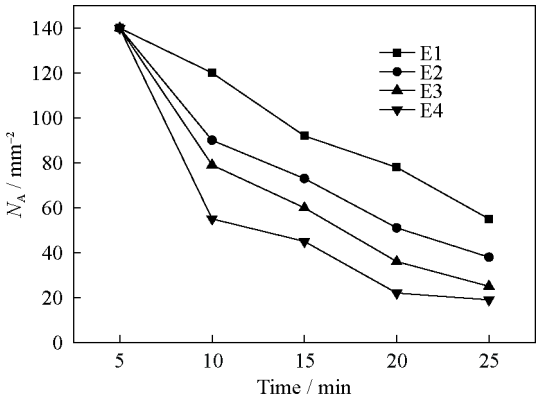

Fig. 5. Change in the number of inclusions larger than 1 μm in different samples.

The total oxygen content in the steel changed significantly, as shown in Fig. 6. As evident in this figure, the total oxygen content in the steel was 0.0060wt%. With increasing experiment time, the total oxygen content in liquid steel decreased continuously. The final total oxygen contents in liquid steel in samples E1, E2, E3, and E4 were 0.0025wt%, 0.0021wt%, 0.0017wt%, and 0.0008wt%, respectively. With increasing magnesium content in liquid steel, the total oxygen content decreased.

The factors that influence inclusion removal by magnesium can be broadly grouped into the following two categories:

(1) In the case of aluminum deoxidation, inclusions in the steel were Al_2O_3 particles, whereas the inclusions were mMgO·$n$$Al_2O_3$ particles in the steel in the case of aluminum–magnesium deoxidation. According to experimental data, the m/n molar ratios were set to 0.5, 1.0, 1.5, and 2.0, respectively. Domanski *et al.* [18] prepared spinels with different magnesia-to-alumina molar ratios and measured the densities of the resulting spinels. The measured densities of the MgO·Al_2O_3 spinels are shown in Table 6. As indicated in this table, the densities of spinel inclusions with different MgO-to-Al_2O_3 molar ratios are in the range 3.92–3.66 g/cm^3; these values are lower than the density of Al_2O_3 (3.97 g/cm^3). Under the same conditions of volume, a lower density of inclusions results in a higher floating rate. It can be concluded that MgO·Al_2O_3 spinels are more easily removed than Al_2O_3 inclusions.

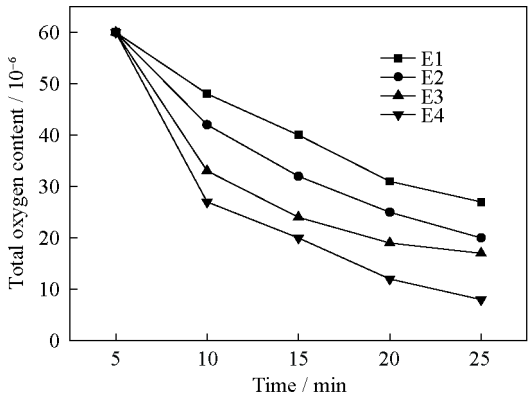

Fig. 6. Change in total oxygen content in different samples.

Table 6. Densities of spinels g·cm^{-3}

$MgO·2Al_2O_3$	$MgO·Al_2O_3$	$1.5MgO·Al_2O_3$	$2MgO·Al_2O_3$
3.92	3.79	3.72	3.66

(2) Because the boiling point of magnesium is low, the addition of magnesium to liquid steel results in the formation of numerous tiny magnesium bubbles. The nitrogen partial pressure in the magnesium bubble is 0 Pa; therefore, nitrogen is transferred from liquid steel into the magnesium bubble until the nitrogen partial pressure in the magnesium bubble reaches the saturation pressure. This phenomenon can be confirmed by the effect of escaping magnesium bubbles on the nitrogen content. As shown in Fig. 7, the nitrogen content in sample E1 decreased with increasing experiment time. This observation can be explained by experiments having been performed under vacuum conditions. The nitrogen contents in samples E2, E3, and E4 also decreased. Thus, increasing magnesium content in liquid steel results in decreased nitrogen content. It indicates that the magnesium bubbles promote nitrogen removal under vacuum conditions.

In addition, magnesium bubbles can stir liquid steel to promote inclusion floating. At the same time, an ongoing deoxidation reaction occurs at the surface of magnesium bubbles. The deoxidation products were finally brought out of liquid steel as magnesium bubbles floated to the liquid-steel surface, which resulted in a decrease in the total oxygen content, as shown in Fig. 6. With increasing magnesium content in liquid steel, additional magnesium bubbles were produced; thus, the number of inclusions along with the number of magnesium bubbles floated was increased.

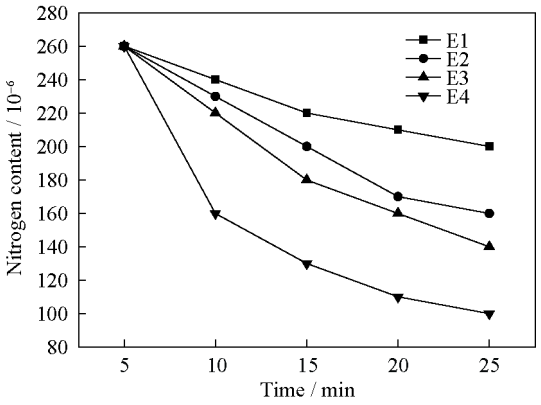

Fig. 7. Change in nitrogen content in steel samples with time.

4. Conclusions

(1) After H13 die steel was deoxidized with the aluminum–magnesium alloy, oxide inclusions in the steel were changed from Al_2O_3 to $MgO{\cdot}Al_2O_3$ and sulfide inclusions were transformed from MnS to MgO·MgS. V(N,C) precipitated around $MgO{\cdot}Al_2O_3$ and MgO·MgS inclusions.

(2) The total oxygen content in H13 steel significantly decreased after aluminum–magnesium deoxidation. The lowest total oxygen content was 0.0008wt%. As the magnesium content in liquid steel was increased, the oxygen content decreased. The density of $MgO{\cdot}Al_2O_3$ inclusions was smaller than that of Al_2O_3 inclusions. As the magnesium content in Mg-containing inclusions increased, the density of inclusions decreased.

(3) The size of inclusions was less than 5 μm in steel deoxidized using aluminum–magnesium. As the magnesium content in liquid steel increased, the number of inclusions larger than 1 μm decreased, whereas the number of inclusions less than 1 μm increased.

Acknowledgements

This work was financially supported by the National Natural Science Foundation of China (No. 51374022) and China Postdoctoral Science Foundation (No. 2014M560047).

References

[1] G.H. Yan, X.M. Huang, Y.Q. Wang, X.G. Qin, M. Yang, Z.M. Chu, and K. Jin, Effects of heat treatment on mechanical properties of H13 steel, *Met. Sci. Heat Treat*., 52(2010), No. 7-8, p. 393.

[2] D. Klobčar, J. Tušek, and B. Taljat, Thermal fatigue of materials for die-casting tooling, *Mater. Sci. Eng. A*, 472(2008), No. 1-2, p. 198.

[3] N. Tripathi and S.C. Du, Chemical characterisation of non-metallic inclusions during casting of hot work die steel, *Ironmaking Steelmaking*, 33(2006), No. 3, p. 213.

[4] F. Chai, C.F. Yang, and H. Su, Effect of magnesium on inclusion formation in Ti-killed steels and microstructural evolution in welding induced coarse-grained heat affected zone, *J. Iron. Steel. Res. Int*.,16(2009), No. 1, p. 69.

[5] V.M. Schastlivtsev, T.I. Tabatchikova, I.L. Yakovleva, and S.Y. Klyueva, Effect of structure and nonmetallic inclusions on the intercrystalline fracture of cast steel, *Phys. Met. Metallogr*., 114(2013), No. 2, p. 180.

[6] J. Yao, X.H. Qu, X.B. He, and L. Zhang, Effect of inclusion size on the high cycle fatigue strength and failure mode of a high V alloyed powder metallurgy tool steel, *Int. J. Miner. Metall. Mater*., 19(2012), No. 7, p. 608.

[7] W.G. Seo, W.H. Han, J.S. Kim, and J.J. Pak, Deoxidation equilibria among Mg, Al and O in liquid iron in the presence of $MgO{\cdot}Al_2O_3$ spinel, *ISIJ Int*., 43(2003), No. 2, p. 201.

[8] R. Takata, J. Yang, and M. Kuwabara, Characteristics of inclusions generated during Al–Mg complex deoxidation of molten steel, *ISIJ Int*., 47(2007), No. 10, p. 1379.

[9] S.J. Luo, Y.H. Su, M.J. Lu, and J.C. Kuo, EBSD analysis of magnesium addition on inclusion formation in SS400 structural steel, *Mater. Charact.*, 82(2013), p. 103.

[10] J.H. Park and H.K. Todoroki, Control of $MgO{\cdot}Al_2O_3$ spinel inclusions in stainless steels, *ISIJ Int*., 50(2010) No. 10, p. 1333.

[11] J. Yang, K.J. Okumura, M. Kuwabara, and M. Sano, Behavior of magnesium in the desulfurization process of molten iron with magnesium vapor produced *in-situ* by aluminothermic reduction of magnesium oxide, *ISIJ Int*., 42(2002), No. 7, p. 685.

[12] C.B. Shi, X.C. Chen, H.J. Guo, Z.J. Zhu, and X.L. Sun, Control of $MgO{\cdot}Al_2O_3$ spinel inclusions during protective gas electroslag remelting of die steel, *Metall. Mater. Trans. B*, 44(2013), No. 2, p. 378.

[13] H. Ohta and H. Suito, Thermodynamics of aluminum and manganese deoxidation equilibria in Fe–Ni and Fe–Cr alloys, *ISIJ Int*., 43(2003), No. 9, p. 1301.

[14] H. Ohta and H. Suito, Calcium and magnesium deoxidation in Fe–Ni and Fe–Cr alloys equilibrated with $CaO–Al_2O_3$ and $CaO–Al_2O_3–MgO$ slags, *ISIJ Int*., 43(2003), No. 9, p. 1293.

[15] K. Fujii, T. Nagasaka, and M. Hino, Activities of the constituents in spinel solid solution and free energies of formation of MgO, $MgO{\cdot}Al_2O_3$, *ISIJ Int*., 40(2000), No. 11, p. 1059.

[16] H. Todoroki and K. Mizuno, Effect of silica in slag on inclusion compositions in 304 stainless steel deoxidized with aluminum, *ISIJ Int*., 44 (2004), No. 8, p. 1350.

[17] A. Hayashi, T. Uenishi, H. Kandori, T. Miki, and M. Hino, Aluminum deoxidation equilibrium of molten Fe–Ni alloy coexisting with alumina or hercynite, *ISIJ Int*., 48(2008), No. 11, p. 1533.

[18] D. Domanski, G. Urretavizcaya, F.J. Castro, and F.C. Gennari, Mechanochemical synthesis of magnesium aluminate spinel powder at room temperature, *J. Am. Ceram. Soc*., 87(2004), No. 11, p. 2020.